Overcoming the underestimation and overestimation problems in adaptive sliding mode control

Roy, Spandan; Roy, Sayan Basu; Lee, Jinoh; Baldi, Simone

DOI
10.1109/TMECH.2019.2930711

Publication date
2019

Document Version
Accepted author manuscript

Published in
IEEE/ASME Transactions on Mechatronics

Citation (APA)
Roy, S., Roy, S. B., Lee, J., & Baldi, S. (2019). Overcoming the underestimation and overestimation problems in adaptive sliding mode control. *IEEE/ASME Transactions on Mechatronics*, *24*(5), 2031-2039. https://doi.org/10.1109/TMECH.2019.2930711

Overcoming the Under- and Over-Estimation Problems in Adaptive Sliding Mode Control

Spandan Roy, Sayan Basu Roy, *Member, IEEE*, Jinoh Lee, *Senior Member, IEEE*, and Simone Baldi, *Member, IEEE*

***Abstract*—Under- and over-estimation problems are commonly observed in conventional adaptive sliding mode control (ASMC). These problems refer to the fact that the adaptive controller gain unnecessarily increases when the states are approaching the sliding surface (overestimation) or improperly decreases when the states are getting far from it (underestimation). In this work, we propose a novel ASMC strategy that overcomes such issues. In contrast to the state of the art, the proposed strategy is effective even when a priori constant bound on the uncertainty cannot be imposed. Comparative results using two-link manipulator demonstrate improved performance as compared to the conventional ASMC. Experimental results on a biped robot confirm the effectiveness and robustness of the proposed method under various practical uncertainties.**

***Index Terms*—Adaptive sliding mode control, underestimation and overestimation, switching gain.**

I. Introduction

A considerable amount of research has been carried out recently on various adaptive-robust control designs (comprising neural network-based designs [1]–[3], switched-based designs [4]–[11], functional observer-based designs [12], [13], time delay-based designs [14]–[16] etc.). Adaptive-robust control aims at reducing structural knowledge of the system like conventional adaptive control, while being intrinsically robust to bounded uncertainties. The most classic form of adaptive-robust control is adaptive sliding mode control adaptive sliding mode control (ASMC) where the control gain (usually referred to in literature as switching gain) is adapted online [4]. Adaptation laws proposed in literature involve monotonically increasing switching gains [5]–[10], whose high gain might cause chattering [17].

A. Background on ASMC

To avoid monotonic behaviour of switching gain, the ASMC laws of [18]–[21] have proposed a threshold-based adaptive law, i.e., the switching gain increases (resp. decreases) when the states are outside (resp. inside) a boundary layer of the sliding surface. Unfortunately, this strategy does not prevent the switching gain which may still be increasing (resp. decreasing) even if the tracking error decreases (resp. increases), leading to *the overestimation (resp. underestimation) problem of switching gain*. Both situations are detrimental to control performance: while the under-estimation problem reduces controller accuracy by applying lower switching gain than the required amount, the over-estimation problem causes larger gain and demands high control input [17]. Similar under- and over-estimation problems arise in the adaptive laws of [22]–[25]. In order to keep the focus on the under- and overestimation problems, our work will be based on the classical first-order ASMC design.

Let us further elaborate on the issues of under- and over-estimation by sketching the problem formulation and open problems. The following notations will be used in this paper: $\lambda_{\min}(\cdot)$, $||\cdot||$ and $(\cdot)^g$ represent the minimum eigenvalue, Euclidean norm and generalised inverse of $(\cdot)$, respectively; $\vee$ and $\wedge$ denote logical 'OR' and 'AND' operators respectively; I denotes identity matrix with appropriate dimension.

B. Motivation

Consider the following class of nonlinear systems, which are suitable to represent many mechatronic systems [26], [27]

$$\ddot{q} = f(q, \dot{q}) + B(q)u, \tag{1}$$

where $q, \dot{q} \in \mathbb{R}^n$ denote positions and velocity; $u \in \mathbb{R}^m$ denotes control input with $m \geq n$; $f : \mathbb{R}^n \times \mathbb{R}^n \mapsto \mathbb{R}^n$ and $B : \mathbb{R}^n \mapsto \mathbb{R}^{n\times m}$ denote the system dynamics terms. The states $x = [q^T \ \dot{q}^T]^T$ are assumed to be measurable. The functions f and B are considered to be uncertain according to the following assumptions:

Assumption 1. *The system dynamics term $f(x)$ can be upper bounded as:*

$$||f(x)|| \leq \theta_0 + \theta_1||x|| + \cdots + \theta_p||x||^p \triangleq Y(x)^T\Theta, \tag{2}$$

where $p \geq 1$; $\theta_i \in \mathbb{R}_0^+$ $i = 0, \cdots, p$ are finite but unknown scalars; $Y(x) = [1 \ ||x|| \ ||x||^2 \ \cdots \ ||x||^p]^T$; $\Theta = [\theta_0 \ \theta_1 \ \theta_2 \ \cdots \ \theta_p]^T$.

Remark 1. *There exist a large class of real-world mechatronic systems such as robotic manipulators [28], [29], mobile robots [30], ship dynamics, aircraft, pneumatic muscles [31] etc.*

This work was partially supported by the "Fundamental Research Funds for The Central Universities" under the project RECON-STRUCT, Grant No. 103009004. (*Corresponding Author: Jinoh Lee.*)

S. Roy is with the Delft Center for Systems and Control (DCSC), Technische Universiteit Delft (TU Delft), Delft, The Netherlands (e-mail: s.roy-2@tudelft.nl).

S. Basu Roy is with Electronics and Communication Engineering, Indraprastha Institute of Information Technology Delhi (IIITD), New Delhi, India (e-mail: sayan@iiitd.ac.in).

J. Lee is with the Advanced Robotics Department, Istituto Italiano di Tecnologia (IIT), Genoa, Italy (e-mail: jinoh.lee@iit.it).

S. Baldi is with the School of Mathematics Southeast University, Nanjing, China and with DCSC, TU Delft, Delft, The Netherlands (e-mail: s.baldi@tudelft.nl).

(in general systems following Lagrangian and Hamiltonian mechanics) where the system dynamics exhibits property (2).

Assumption 2. *The nominal value of $B(x)$, call it $\hat{B}(x)$, is selected such that for a known scalar E the following holds*

$$||B(x)\hat{B}(x)^g - I|| \triangleq E < 1. \tag{3}$$

Remark 2. *Assumption 2 implies that the perturbation in $B(x)$ cannot be more than that of the nominal input matrix $\hat{B}(x)$. Such an uncertainty description is typically adopted and can be satisfied for many practical electro-mechanical systems [27, §11].*

Let $q^d(t)$, the desired trajectory to be tracked, be selected such that $q^d, \dot{q}^d, \ddot{q}^d \in \mathcal{L}_\infty$. Let $e(t) \triangleq q(t) - q^d(t)$ be the tracking error and s be the sliding surface designed as:

$$s \triangleq \dot{e} + \Omega e \Rightarrow s = \Gamma\xi, \tag{4}$$

where $\Gamma \triangleq [\Omega\ I]$, $\xi \triangleq [e^T\ \dot{e}^T]^T$ and $\Omega \in \mathbb{R}^{n\times n}$ is a positive definite matrix. Using (1), the time derivative of (4) yields

$$\begin{aligned}\dot{s} = \ddot{q} - \ddot{q}^d + \Omega\dot{e} &= f(x) - \ddot{q}^d + \Omega\dot{e} + B(x)u \\ &= \Psi(x,\xi) + B(x)u,\end{aligned} \tag{5}$$

where $\Psi(x,\xi) \triangleq f(x) - \ddot{q}^d + \Omega\dot{e}$, referred as *system uncertainty* hereafter. As $n \leq m$, the system uncertainty satisfies the matching condition in Assumption 2. Similar assumption on uncertainties is implicit in most ASMC literature (cf. [18], [19], [21]–[23]); however, because the uncertainty is state-dependent, one cannot use the tools from literature which require uncertainties to be bounded a priori. Application of ARC for the case $n > m$ avoiding structural constraint is to the best of the authors' knowledge open and can be a future research direction.

The following two observations mark the difference between the conventional ASMC as well as the goals.

Observation 1: The overestimation-underestimation problem of conventional ASMC can be easily illustrated via the adaptive law of [18], [19] as an example:

$$\dot{K} = \begin{cases}\bar{K}||s||\text{sgn}(||s|| - \epsilon), & \text{if } K > \bar{\epsilon} \\ \bar{\epsilon} & \text{if } K \leq \bar{\epsilon}\end{cases} \qquad \epsilon = 4KT_s, \tag{6}$$

where $\bar{K}, \bar{\epsilon} \in \mathbb{R}^+$ are user defined scalars, ϵ is a *time-varying threshold value* and T_s is the discretization time (cf. [18], [19] for detailed structure of the control law). It can be observed from (6) that when $||s|| > \epsilon$ (resp. $||s|| < \epsilon$), the switching gain K increases (resp. decreases) monotonically even if the error trajectories move close to (resp. move away from) $||s|| = 0$. This gives rise to the overestimation (resp. underestimation) problem of switching gain. Similar problems also arise in the adaptive laws of [20]–[25].

Observation 2: State-of-the-art ASMC works either assume that $||\Psi||$ ([5]–[10], [18]–[21], [32]) or its time derivative ([22]–[24]) is upper bounded by a constant, a priori. The upper bound structure of $||f||$ in (2) reveals that a constant bound assumption on $||\Psi||$ or on its time derivative imposes an a priori bound on the states (i.e., before analysing closed-loop stability), which is a restrictive assumption.

C. Contribution

In view of the pertaining issues of the state-of-the-art, as highlighted in **Observations 1-2**, the main contribution of this work is a novel ASMC framework that, as compared to [18]–[21], [23]–[25], stops increasing (resp. decreasing) the control gain when the tracking error decreases (resp. increases). Thanks to this strategy, the proposed framework avoids the overestimation-underestimation problems of switching gain.

The remainder of the work is organized as follows: The proposed ASMC framework is designed in Section II along with its detailed stability analysis; Section III presents a case study with comparative simulation results, Section IV presents experimental validation of the proposed ASMC using cCub biped robot [33]; Section V presents concluding remarks.

II. Proposed ASMC Formulation

The control input of the proposed ASMC is designed as

$$u = \hat{B}^g(-\Lambda s - \Delta u),\ \Delta u = \zeta\rho\ sat(s,\varpi), \tag{7}$$

where Λ is a positive definite matrix; $\zeta \geq 1$ is a user-defined scalar; $sat(\cdot,\cdot)$ is the standard 'saturation' function defined as $sat(s,\varpi) = s/||s||$ (resp. s/ϖ) if $||s|| \geq \varpi$ (resp. $||s|| < \varpi$); $\varpi \in \mathbb{R}^+$ is a small scalar used to avoid chattering [34]. The gain term ρ will be defined later. Substituting (7) in (5) and then adding and subtracting $(\Lambda s + \Delta u)$, the closed-loop dynamics is formed as:

$$\begin{aligned}\dot{s} &= \Psi - (B\hat{B}^g - I)(\Lambda s + \Delta u) - \Lambda s - \Delta u \\ &= \upsilon - (B\hat{B}^g - I)\Delta u - \Lambda s - \Delta u,\end{aligned} \tag{8}$$

where $\upsilon \triangleq \Psi - (B\hat{B}^g - I)\Lambda s$. Since $\xi = [e^T\ \dot{e}^T]^T$, then $||\xi|| \geq ||e||, ||\xi|| \geq ||\dot{e}||$. Using $x = \xi + \begin{bmatrix}q^d \\ \dot{q}^d\end{bmatrix}$, the following relation holds from (2):

$$||\upsilon|| \leq \theta_0^* + \theta_1^*||\xi|| + \cdots + \theta_p^*||\xi||^p \triangleq Y(\xi)^T\Theta^*, \tag{9}$$

where $\theta_i^* \in \mathbb{R}^+\ i = 0,\cdots,p$ are finite but unknown scalars; $Y(\xi) = [1\ ||\xi||\ ||\xi||^2\ \cdots\ ||\xi||^p]^T$; $\Theta^* = [\theta_0^*\ \theta_1^*\ \theta_2^*\ \cdots\ \theta_p^*]^T$.

The term ρ in (7) is designed as follows:

$$\begin{aligned}\rho &= \frac{1}{1-E}(\hat{\theta}_0 + \hat{\theta}_1||\xi|| + \cdots + \hat{\theta}_2||\xi||^p) \\ &\triangleq \frac{1}{1-E}(Y(\xi)^T\hat{\Theta}),\end{aligned} \tag{10}$$

where $\hat{\Theta} = [\hat{\theta}_0\ \hat{\theta}_1\ \cdots\ \hat{\theta}_p]^T$ is the estimate of Θ^*. The gains $\hat{\theta}_i$, $i = 0,1,\cdots,p$ are evaluated as:

$$\dot{\hat{\theta}}_i = \begin{cases}\alpha_i||\xi||^i||s|| & \text{if } (\sigma(s) > 0) \vee (\bigcup_{i=0}^p \hat{\theta}_i \leq 0) \\ -\underline{\alpha}_i||\xi||^i||s|| & \text{if } (\sigma(s) \leq 0) \wedge (\bigcap_{i=0}^p \hat{\theta}_i > 0)\end{cases} \tag{11}$$

$$\text{with } \hat{\theta}_i(t_0) > 0, i = 0,1,\cdots,p, \tag{12}$$

where t_0 is the initial time; $\alpha_i, \underline{\alpha}_i \in \mathbb{R}^+$ are user-defined scalars; $\sigma(s)$ is a user-defined function, designed in a way to guarantee $\sigma(s) > 0$ (resp. $\sigma(s) \leq 0$) whenever $||s||$ increases (resp. does not increase). In view of the fact that, in practice, one can only obtain feedback data for sensors at sampling intervals T_s, a relevant choice for $\sigma(s)$ becomes $\sigma(s) = ||s(t)|| - ||s(t - T_s)||$. The notations '$\bigcup_{i=0}^p \hat{\theta}_i$' and

'$\bigcap_{i=0}^{p}\hat{\theta}_i$' respectively signify 'either of $\hat{\theta}_i$' and 'all $\hat{\theta}_i$' for $i=0,\cdots,p$.

Remark 3. *The initial condition of the gains are selected as $\hat{\theta}_i(t_0)>0$. Note that the first adaptive law in (11) forces the gains to increase if at least one gain tends to go negative (i.e., $(\bigcup_{i=0}^{p}\hat{\theta}_i\leq 0)$). This ensures that*

$$\hat{\theta}_i(t)\geq 0\ \forall i=0,1,\cdots,p\quad \forall t\geq t_0. \tag{13}$$

A. Stability Analysis of the Proposed ASMC

Theorem 1. *Under Assumptions 1 and 2, the closed-loop system (8) with control input (7), (10) and adaptive law (11) guarantees $\xi(t), s(t), \tilde{\theta}_i(t)$ to be Uniformly Ultimately Bounded (UUB).*

Proof. The stability analysis is carried out using the following Lyapunov function:

$$V=\frac{1}{2}s^Ts+\sum_{i=0}^{p}\frac{\tilde{\theta}_i^2}{2\alpha_i}, \tag{14}$$

where $\tilde{\theta}_i\triangleq(\hat{\theta}_i-\theta_i^*)$, $i=0,1,\cdots,p$. Exploring the structures of $sat(s,\varpi)$ in (7) and of the adaptive law (11), four possible cases can be identified:

- Case (1): $\dot{\hat{\theta}}_i>0\ \forall i=0,1,\cdots,p$ and $||s||\geq\varpi$;
- Case (2): $\dot{\hat{\theta}}_i<0\ \forall i=0,1,\cdots,p$ and $||s||\geq\varpi$;
- Case (3): $\dot{\hat{\theta}}_i>0\ \forall i=0,1,\cdots,p$ and $||s||<\varpi$;
- Case (4): $\dot{\hat{\theta}}_i<0\ \forall i=0,1,\cdots,p$ and $||s||<\varpi$.

The closed-loop system stability is analysed for these four cases using the common Lyapunov function (14).

Case (1): $\hat{\theta}_i$ increase $\forall i=0,1,\cdots,p$ and $||s||\geq\varpi$.

Note that $\sum_{i=0}^{p}\frac{1}{\alpha_i}\tilde{\theta}_i\dot{\hat{\theta}}_i=Y(\xi)^T(\hat{\Theta}-\Theta^*)||s||$. Then using (8)-(11) one obtains

$$\begin{aligned}\dot{V}&=s^T\dot{s}+Y(\xi)^T(\hat{\Theta}-\Theta^*)||s||\\&=s^T(\upsilon-(B\hat{B}^g-I)\Delta u-\Lambda s-\Delta u)\\&\qquad+Y(\xi)^T(\hat{\Theta}-\Theta^*)||s||\\&\leq -s^T\Lambda s-\zeta(1-E)\rho||s||+s^T\upsilon+Y(\xi)^T(\hat{\Theta}-\Theta^*)||s||\\&\leq -s^T\Lambda s-Y(\xi)^T(\hat{\Theta}-\Theta^*)||s||+Y(\xi)^T(\hat{\Theta}-\Theta^*)||s||\\&\leq -\lambda_{\min}(\Lambda)||s||^2\leq 0.\end{aligned} \tag{15}$$

From (15) it can be inferred that V is bounded for this case, implying boundedness of $\tilde{\theta}_i$ and s. This in turn ensures boundedness of $e,\dot{e}$ and $\hat{\theta}_i$. Therefore, $\exists\ \bar{\theta}_i\in\mathbb{R}^+$ such that

$$\hat{\theta}_i(t)\leq\bar{\theta}_i\ ,\ i=0,1,\cdots,p \text{ when } ||s||\geq\varpi. \tag{16}$$

Note that $\dot{\hat{\theta}}_i>0$ implies the gains $\hat{\theta}_i$ will increase. Thus, to avoid overestimation, we have to prove that (11) provides a mechanism such that the estimates would stop increasing after a finite time so that Case (2) is initiated. Since, $\dot{\hat{\theta}}_i>0\Rightarrow||s||>0$ (from (11)), there always exists $0<\delta<\varpi$ such that $||s||\geq\delta$. Hence, $s=\Gamma\xi$ yields

$$\delta\leq||s||\leq||\Gamma||||\xi||\Rightarrow||\xi||\geq(\delta/||\Gamma||). \tag{17}$$

Using (17), the first law of (11) yields

$$\dot{\hat{\theta}}_i\geq\alpha_i\delta(\delta/||\Gamma||)^i,\quad i=0,1,\cdots,p. \tag{18}$$

Taking $V_1=(1/2)s^Ts$ and following the simplifications in (15), one has

$$\begin{aligned}\dot{V}_1&\leq -s^T\Lambda s-Y(\xi)^T\hat{\Theta}||s||+Y(\xi)^T\Theta^*||s||\\&\leq -\lambda_{\min}(\Lambda)||s||^2-\sum_{i=0}^{p}(\hat{\theta}_i-\theta_i^*)||\xi||^i||s||.\end{aligned} \tag{19}$$

According to the second law of (11), the gains start to decrease if $s^T\dot{s}\leq 0$ and $\hat{\theta}_i>0\ \forall i$. Thus, when $\hat{\theta}_i\geq\theta_i^*\ \forall i$, one has $\dot{V}_1=s^T\dot{s}<0$ from (19) and the gains start decreasing. Now, integrating both sides of (18) one can find that $\hat{\theta}_i\geq\theta_i^*$ will be satisfied within the finite times

$$t_{ri}\leq(1/\alpha_i\delta)(||\Gamma||/\delta)^i\quad\forall i=0,1,\cdots,p. \tag{20}$$

Thus, the gains would start to decrease at $t\geq T$ where $T\leq\bar{t}$ and $\bar{t}=\max\{t_{r0},t_{r1},\cdots,t_{rp}\}$.

Case (2): $\hat{\theta}_i$ decrease $\forall i=0,1,\cdots,p$ and $||s||\geq\varpi$.

Using $\hat{\theta}_i\geq 0$ (from (13)) and $||s||\leq||\Gamma||||\xi||$ yields:

$$\begin{aligned}\dot{V}&=s^T(\upsilon-(B\hat{B}^g-I)\Delta u-\Lambda s-\Delta u)\\&\qquad-(\underline{\alpha}_i/\alpha_i)Y(\xi)^T(\hat{\Theta}-\Theta^*)||s||\\&\leq -s^T\Lambda s-Y(\xi)^T(\hat{\Theta}-\Theta^*)||s||\\&\qquad-(\underline{\alpha}_i/\alpha_i)Y(\xi)^T(\hat{\Theta}-\Theta^*)||s||\\&\leq -\lambda_{\min}(\Lambda)||s||^2+(1+\underline{\alpha}_i/\alpha_i)||\Gamma||\{\theta_0^*+\theta_1^*||\xi||+\theta_2^*||\xi||^2\\&\qquad+\cdots+\theta_p^*||\xi||^p\}||\xi||.\end{aligned} \tag{21}$$

Note that the condition $\{(\sigma(s)\leq 0)\wedge(\bigcap_{i=0}^{p}\hat{\theta}_i>0)\}$ is necessary to establish Case (2) which means $\sigma(s)\leq 0$ is one of the required condition to be satisfied. Further, $\sigma(s)\leq 0$ implies $||s||$ does not grow in Case (2), i.e., $\exists\beta\in\mathbb{R}^+$ such that $||s||\leq\beta$ in this case. Hence, using the relation $s=\Gamma\xi$, the followings are satisfied for Case (2):

$$||s||\leq\beta\Rightarrow||\Gamma\xi||\leq\beta. \tag{22}$$

Moreover, (22) implies $\exists\gamma\in\mathbb{R}^+$ such that

$$\begin{aligned}(1+\underline{\alpha}_i/\alpha_i)||\Gamma||(\theta_0^*+\theta_1^*||\xi||+\theta_2^*||\xi||^2+\\\cdots+\theta_p^*||\xi||^p)||\xi||\leq\gamma.\end{aligned} \tag{23}$$

Substitution of (23) into (21) yields

$$\dot{V}\leq-\lambda_{\min}(\Lambda)||s||^2+\gamma. \tag{24}$$

Since $0\leq\hat{\theta}_i(t)\leq\bar{\theta}_i$ (from (13) and (16)), the definition of V in (14) yields

$$V\leq||s||^2+\chi\Rightarrow-||s||^2\leq-V+\chi, \tag{25}$$

where $\chi\triangleq\sum_{i=0}^{p}\frac{1}{\alpha_i}(\theta_i^{*2}+\bar{\theta}_i^{\,2})$.

Let us define a scalar z as $0<z<\lambda_{\min}(\Lambda)$. Then taking $\varrho\triangleq(\lambda_{\min}(\Lambda)-z)$ and using (25), (24) can be modified as

$$\begin{aligned}\dot{V}&\leq-\{\lambda_{\min}(\Lambda)-z\}||s||^2-z||s||^2+\gamma\\&=-\varrho V-z||s||^2+\varrho\chi+\gamma\end{aligned} \tag{26}$$

Hence, decreasing V can be derived when

$$||s||=||\Gamma\xi||\geq\sqrt{(\varrho\chi+\gamma)/z}\triangleq\iota. \tag{27}$$

That is, V decreases when $||s||\geq\iota$ and reaches within a set $\Omega_l\triangleq\{V(s,\tilde{\theta}_i)\leq\bar{\iota}:||s||<\iota\}$ within a finite time and stays

there [35]. This also implies that there exist a set Ω_u and scalar $c > \bar{\iota}$ such that $\Omega_u \triangleq \{V(s,\tilde{\theta}_i) \leq c : ||s|| \geq \iota\}$. The definition of V yields $V \geq (1/2)||s||^2 \triangleq \kappa$. Since Case (2) starts within a finite time, let $t = T_0$ be its initial time. Then $||s||$ reaches ι within a finite time duration $[T_0 \;\; T_0 + (c-\bar{\iota})/\varrho\kappa]$ [35].

Case (3): $\hat{\theta}_i$ increase, $\forall i = 0, 1, \cdots, p$ when $||s|| < \varpi$. Similar to Case (1), $\dot{V}$ can be simplified for this case as

$$\begin{aligned}\dot{V} &= -s^T\Lambda s + s^T(-\zeta\rho(s/\varpi) + \upsilon - (B\hat{B}^g - I)\Delta u) \\ &\qquad + Y(\xi)^T(\hat{\Theta} - \Theta^*)||s|| \\ &= -s^T\Lambda s - Y(\xi)^T\hat{\Theta}(||s||^2/\varpi) + Y(\xi)^T\Theta^*||s|| \\ &\qquad + Y(\xi)^T(\hat{\Theta} - \Theta^*)||s|| \\ &\leq -\lambda_{\min}(\Lambda)||s||^2 + Y(\xi)^T\hat{\Theta}||s||. \end{aligned} \tag{28}$$

As $\delta < \varpi$ (from Case (1)), thus using the condition $\delta \leq ||s|| < \varpi$ for Case (3) one has

$$\begin{aligned}\dot{V}_1 &\leq -s^T\Lambda s - Y(\xi)^T\hat{\Theta}(||s||^2/\varpi) + Y(\xi)^T\Theta^*||s|| \\ &\leq -\lambda_{\min}(\Lambda)||s||^2 - \sum_{i=0}^{p}((\hat{\theta}_i(\delta/\varpi) - \theta_i^*)||\xi||^i)||s||. \end{aligned} \tag{29}$$

Following the similar arguments like in Case (1), one can infer for Case (3) that, $(\hat{\theta}_i(\delta/\varpi) \geq \theta_i^*$ would occur at $t \geq T'$ where $T' \leq \bar{t}'$ and $\hat{\theta}_i$'s would start to decrease initiating Case (4). Here, $\bar{t}' = \max\{t'_{r0}, t'_{r1}, \cdots, t'_{rp}\}$ such that

$$t'_{ri} \leq (1/\alpha_i\delta)(\varpi/\delta)(||\Gamma||/\delta)^i \quad \forall i = 0, 1, \cdots, p. \tag{30}$$

The integral of a piecewise continuous function over a finite duration is finite [36]. Since $\hat{\theta}_i$ is piecewise continuous (from (11)) and gains only increase for finite time upto $\bar{t}'$, $\hat{\theta}_i$'s remain finite and thus bounded for Case (3). For $||s|| < \varpi$, system remains bounded inside the ball $B_\varpi \triangleq \{b_\varpi : b_\varpi = ||\Gamma\xi|| < \varpi\}$ as $s = \Gamma\xi$. This implies that $\xi \in \mathcal{L}_\infty \Rightarrow Y(||\xi||) \in \mathcal{L}_\infty$. Further, boundedness of $\hat{\theta}_i$'s and ξ imply $\rho \in \mathcal{L}_\infty$. Hence, for $||s|| < \varpi$, $\exists\vartheta \in \mathbb{R}^+$ such that

$$||Y(\xi)^T\hat{\Theta}||||s|| \leq \varpi\vartheta. \tag{31}$$

Following (26) and using (31), (28) is modified as

$$\dot{V} \leq -\varrho V - z||s||^2 + \varrho\chi + \varpi\vartheta. \tag{32}$$

Hence, decreasing V can be derived when

$$||s|| = ||\Gamma\xi|| \geq \sqrt{(\varrho\chi + \varpi\vartheta)/z}. \tag{33}$$

Case (4): $\hat{\theta}_i$ decrease, $\forall i = 0, 1, \cdots, p$ when $||s|| < \varpi$. Proceeding like Case (3), $\dot{V}$ can be simplified here as

$$\begin{aligned}\dot{V} &\leq -s^T\Lambda s - \zeta Y(\xi)^T\hat{\Theta}(||s||^2/\varpi) + Y(\xi)^T\Theta^*||s|| \\ &\qquad - Y(\xi)^T(\hat{\Theta} - \Theta^*)||s|| \\ &\leq -\lambda_{\min}(\Lambda)||s||^2 + (1 + \underline{\alpha}_i/\alpha_i)||\Gamma||(\theta_0^* + \theta_1^*||\xi|| \\ &\qquad + \theta_2^*||\xi||^2 + \cdots + \theta_p^*||\xi||^p)||\xi||. \end{aligned} \tag{34}$$

This case along with finite time reachability can be analysed exactly like Case (2) and thus, the repetition is avoided. The UUB results for $||s|| \geq \varpi$ and $||s|| < \varpi$ using the common Lyapunov function (14) imply that the overall closed-loop system also remains UUB [37] as well as $e, \dot{e}$ remain bounded.

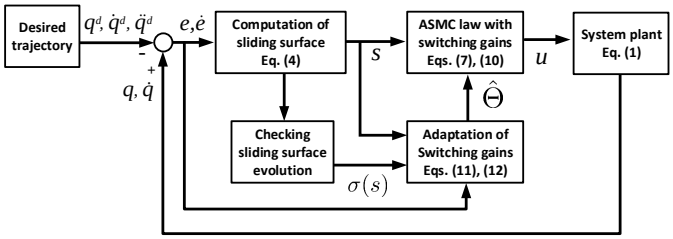

Figure 1. The block diagram of the proposed ASMC.

We finally notice that all the scalars $\delta, \iota, \vartheta, \gamma, \beta, \chi, z, \varrho$ and $\bar{\theta}_i$ were introduced only for the purpose of analysis and not for designing the control law. □

A block diagram of the proposed ASMC law is illustrated in Fig. 1, and some remarks follow:

Remark 4. *The main purpose of verifying the condition $\sigma(s) > 0$ (resp. $\sigma(s) \leq 0$) in (11) is to check whether the error trajectories are moving away from (resp. moving towards) the sliding surface and adapt the gains accordingly to overcome the over- and under-estimation problems. Specifically, the condition $\sigma(s) > 0$ (resp. $\sigma(s) \leq 0$) is utilized to construct (17) (resp. (22)) leading to the derivation of (20) (resp. (23)).*

Remark 5. *The proposed stability result does not impose any restriction on the choice of the scalars α_i and $\underline{\alpha}_i$ in (11) as long as they are positive. However, proper tuning might be beneficial to performance balance, as these parameters decide the adaptation rates for the switching gains $\hat{\theta}_i$ leading to a trade off between tracking accuracy (high gain) and reduced control effort (low gain). Therefore, a designer can select these gains according to application requirements.*

III. Case Study: Euler-Lagrange Systems

Euler-Lagrange (EL) systems have immense applications in various domains such as defence, automation industry, surveillance, space missions etc. , and are a class of systems where Assumption 1 and 2 are intrinsically or easily satisfied. Therefore, it is relevant to see how the proposed design can be recast in such a case study. In general, a second-order EL system has the following system dynamics [26, §2]

$$M(q)\ddot{q} + C(q,\dot{q})\dot{q} + G(q) + F(\dot{q}) + d = u, \tag{35}$$

where $M(q) : \mathbb{R}^n \mapsto \mathbb{R}^{n\times n}$ represents mass/inertia matrix, $C(q,\dot{q}) : \mathbb{R}^n \times \mathbb{R}^n \mapsto \mathbb{R}^{n\times n}$ denotes Coriolis, centripetal terms, $G(q) : \mathbb{R}^n \mapsto \mathbb{R}^n$ denotes gravity vector, $F(\dot{q}) : \mathbb{R}^n \mapsto \mathbb{R}^n$ represents the vector of damping and friction forces; $u \in \mathbb{R}^n$ is the control input and $d(t)$ denotes the bounded external disturbances. The system (35) possesses the following properties [27]:

Property 1. *$\exists C_b, G_b, F_b, \bar{d} \in \mathbb{R}^+$ such that $||C(q,\dot{q})|| \leq C_b||\dot{q}||$, $||G(q)|| \leq G_b$, $||F(\dot{q})|| \leq F_b||\dot{q}||$ and $||d(t)|| \leq \bar{d}$.*

Property 2. *The matrix $M(q)$ is uniformly positive definite and there exist two positive constants μ_1, μ_2 such that*

$$0 < \mu_1 I \leq M(q) \leq \mu_2 I. \tag{36}$$

Representing the system dynamics (35) as (1), one has

$$f(q,\dot{q}) = -M^{-1}(q)\{C(q,\dot{q})\dot{q} + G(q) + F(\dot{q}) + d\}, \quad (37a)$$
$$B(q) = M^{-1}(q). \quad (37b)$$

The vector $x = [q^T \ \dot{q}^T]^T$ implies $||x|| \geq ||q||, ||x|| \geq ||\dot{q}||$. Thus, using the ***Properties*** 1 and 2, one has

$$\begin{aligned} ||f|| &\leq (1/\mu_1)(C_b||\dot{q}||^2 + F_b||\dot{q}|| + G_b + \bar{d}) \\ &\leq (1/\mu_1)(C_b||x||^2 + F_b||x|| + G_b + \bar{d}) \\ &\triangleq \theta_0 + \theta_1||x|| + \theta_2||x||^2, \end{aligned} \quad (38)$$

where $\theta_0 = (1/\mu_1)(G_b + \bar{d}), \theta_1 = (1/\mu_1)F_b, \theta_2 = (1/\mu_1)C_b$. Thus, the EL system (35) intrinsically verifies Assumption 1 with $p = 2$. Hence, the control structure of the proposed ASMC for EL system (35) consists of (7), (10)-(12) with $p = 2$.

A. Application: 2-Link Manipulator

1) Simulation scenario: The two-link manipulator under consideration has dynamics in the form (35), with

$$M = \begin{bmatrix} M_{11} & M_{12} \\ M_{12} & M_{22} \end{bmatrix}, q = \begin{bmatrix} q_1 \\ q_2 \end{bmatrix},$$
$$M_{11} = (m_1 + m_2)l_1^2 + m_2 l_2(l_2 + 2l_1\cos(q_2)),$$
$$M_{12} = m_2 l_2(l_2 + l_1\cos(q_2)), M_{22} = m_2 l_2^2,$$
$$C = \begin{bmatrix} -m_2 l_1 l_2 \sin(q_2)\dot{q}_2 & -m_2 l_1 l_2 \sin(q_2)(\dot{q}_1 + \dot{q}_2) \\ m_2 l_1 l_2 \sin(q_2)\dot{q}_1 & 0 \end{bmatrix},$$
$$G = \begin{bmatrix} m_1 l_1 g\cos(q_1) + m_2 g(l_2\cos(q_1 + q_2) + l_1\cos(q_1)) \\ m_2 g l_2 \cos(q_1 + q_2) \end{bmatrix},$$
$$F = \begin{bmatrix} f_{v1} sgn(\dot{q}_1) \\ f_{v2} sgn(\dot{q}_2) \end{bmatrix}, d = \begin{bmatrix} 0.5\sin(0.5t) \\ 0.5\sin(0.5t) \end{bmatrix}.$$

Here (m_1, l_1, q_1) and (m_2, l_2, q_2) denote the mass, length and position of link 1 and 2 respectively. The following parametric values are selected for simulation: $l_1 = 0.6$m, $l_2 = 0.3$m, $f_{v1} = 0.5, f_{v2} = 0.6, g = 9.8$m/s^2. Apart from the external disturbance d, a sinusoidal uncertainty is considered in mass for both the links, i.e., $m_1 = (5 + 0.5abs(\sin(t)))$kg, $m_2 = (2.5 + 0.5abs(\sin(t)))$kg are considered in simulation (here $abs(\cdot)$ denotes absolute value). The manipulator should track the desired trajectories $q_1^d(t) = q_2^d(t) = \sin(t)$.

The proposed ASMC is compared with that proposed in [18], [19], i.e. the adaptive law (6). This will be denoted as cASMC (conventional ASMC) for compactness. It is to be noted that cASMC requires the knowledge of the nominal values of M, C, G and F, while the proposed ASMC only requires the nominal knowledge of M. Nominal knowledge is obtained by selecting the nominal values $\hat{m}_1 = 5$kg, $\hat{m}_2 = 2.5$kg, $\hat{l}_1 = 0.5$m, $\hat{l}_2 = 0.25$m, $\hat{f}_{v1} = 0.4, \hat{f}_{v2} = 0.5$.

During simulation, the following controller parameters are selected for the proposed ASMC: $\Lambda = 5I, \Omega = I, \varpi = 0.1$, $\hat{\theta}_i(0) = 20$, $\zeta = 4, \alpha_i = \underline{\alpha}_i = 10 \ \forall i = 0, 1, 2$ and $\sigma(s) = ||s(t)|| - ||s(t - T_s)||$. Further, it is found that Assumption 2 holds with $E = 0.412$ while considering the nominal values and perturbations in m_1, m_2. The controller parameters for cASMC are selected as $\bar{K} = 10, \bar{\epsilon} = 0, K(0) = 60$. Finally, sliding variable as in (4), initial state as $q_1(0) = q_2(0) = 0.1$rad and $T_s = 0.001$s are set for both the controllers for parity.

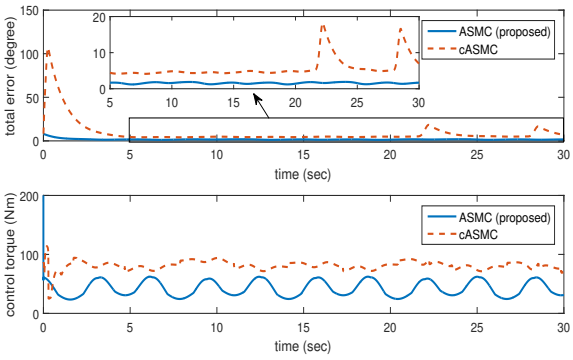

Figure 2. Tracking performance comparison between ASMC (proposed) and cASMC.

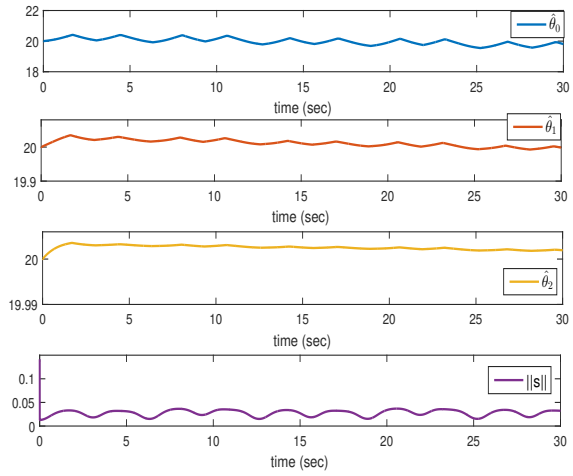

Figure 3. Switching evaluation of the proposed ASMC with $||s||$.

2) Simulation Results and Comparison: The performance of the proposed AMSC and that of cASMC are compared in Fig. 2 in terms of (i) total error (defined as the Euclidean distance in the tracking error of Links 1 and 2) and (ii) control torque (defined as the 1-norm of u).

To clarify the contribution of the proposed ASMC in overcoming the over- and under-estimation problems, the switching gain plots for ASMC and cASMC are provided in Figs. 3 and 4 respectively. Figure 3 illustrates the evolutions of the gains $\hat{\theta}_0, \hat{\theta}_1, \hat{\theta}_2$ with respect to the variations in $||s||$: this substantiates the observation in Remark 4 that all the gains (i.e., $\hat{\theta}_0, \hat{\theta}_1, \hat{\theta}_2$) follow the pattern of $||s||$ (i.e. they increase when $||s||$ increases and decrease when $||s||$ decreases). On the other hand, it is to be noted from Fig. 4 that the switching gain K of cASMC increases even when $||s||$ approaches towards zero for the time intervals t=0.12−0.30s, t=22.02−22.27s, t=28.30−28.56s etc. This is due to the fact that K cannot decrease unless $||s|| < \epsilon$ and this gives rise to the *overestimation* problem (cf. the unnecessarily high peak of K at around 0.3s). According to (6), K decreases monotonically when $||s|| < \epsilon$ for example during t=1.00−20.00s, t=22.24−27.94s etc. This

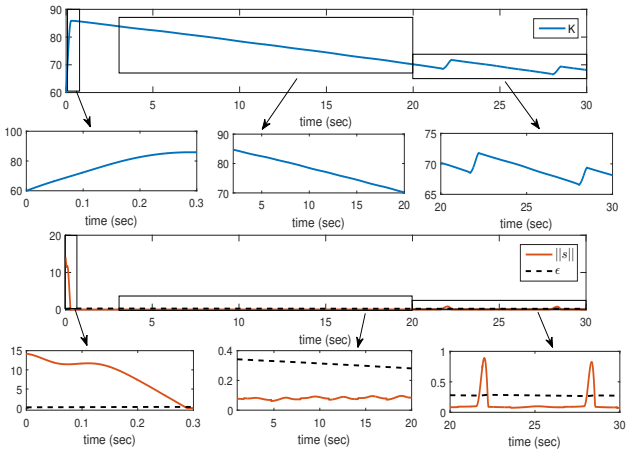

Figure 4. Switching gain evaluation of cASMC.

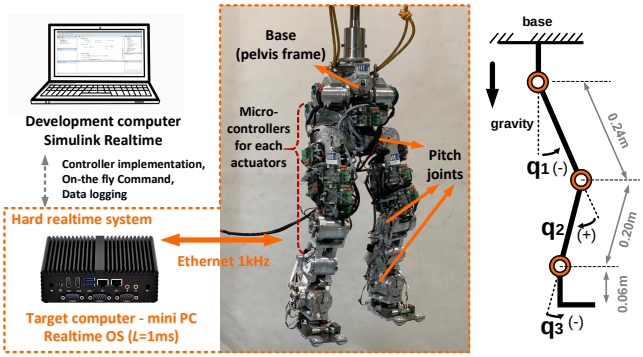

Figure 5. The experimental setup of the cCub robot with the realtime control system, and the schematic diagram of its kinematic structure.

happens despite the fact that during these time intervals, $||s||$ increases several times. As a matter of fact, this gives rise to the *underestimation* problem: because K becomes smaller and insufficient to tackle uncertainties, it occurs that the trajectories will suddenly go away from the sliding surface (cf. the spikes at around 22s and 28s and the corresponding spiking error in Fig. 2), whereas $||s||$ in Fig. 3 and the corresponding error in Fig. 2 stabilize to some ultimate bound.

It can be noted from (11) that while increment-decrement of $\hat{\theta}_0$ solely depends on the value of $||s||$, the same for $\hat{\theta}_1$ and $\hat{\theta}_2$ depend on both $||s||$ as well as $||\xi||$. Hence, noting the relation (4) and the low tracking error (cf. the error plots in Fig. 2), it can be realized from Fig. 3 that variations in $\hat{\theta}_1$ and $\hat{\theta}_2$ are comparatively smaller compared to $\hat{\theta}_0$.

IV. Experimental Results and Analysis

The experimental setup is depicted in Fig. 5. To demonstrate the effectiveness and robustness of the proposed ASMC in a real-life system, it is experimented on a biped robot setup, named cCub [33]. Each leg of the robot has six degrees-of-freedom (DoFs), thus making a total of twelve DoFs for the whole robot. The kinematic structure of the leg is with pitch-roll-yaw joints at the hip, and pitch joints at the knee, and pitch-roll joints at the ankle. The robot weighs 17.3kg in total, while the link lengths are 0.24m from the hip to the knee, 0.20m from knee to the ankle, and 0.06m from the ankle to the foot sole. All joints are equally equipped with a BLDC motor (Kollmorgen RBE series) and a harmonic gear (Harmonic Drive CSG series) with a gear ratio of 100:1, which generates peak torques up to 40 Nm. Since the robot angle of the motor is measured by a magnetic absolute encoder with a resolution of 12-bit, the ultimate resolution of the joint angle (q) after the gear reduction is 0.879×10^{-3} in degrees.

For experimental purposes, the robot is considered as a manipulator with dynamics shown in (35), where the three pitch joints (in the sagittal plane) hip (q_1), knee (q_2) and ankle joints (q_3), are controlled while other joints are kept fixed at zero angles. Thus, six pitch joints of two legs are simultaneously operated. Each joint is controlled by an embedded microcontroller with a sampling rate of 1 kHz which generates the control torque (u) and reads the joint angle (q). The proposed controller is implemented in the realtime control system using Simulink Real-Time™ which communicates with the microcontrollers of the robot in every 1ms.

Note that the experimental implementation of cASMC is very difficult for the cCub robot, as only nominal values and approximate upper-bounds of M are available [33], while cASMC also requires nominal knowledge of C, F and G which are uncertain and significantly time-varying for the cCub robot. This, in our opinion, also highlights the effectiveness of the proposed ASMC scheme in dealing with unknown uncertainties for a complex system like cCub.

To properly judge the performance of the proposed controller, two experimental scenarios, S1 and S2, are considered in following subsections. For both S1 and S2, the control design parameters are: $\Lambda = \Omega = 20I$, $\zeta = 2$, $\varpi = 0.2, \alpha_i = \underline{\alpha}_i = 10, \hat{\theta}_i(0) = 20\ i = 0, 1, 2$, $\sigma(s) = ||s(t)|| - ||s(t - T_s)||$ and $T_s = 0.001$. For simplicity, $\hat{B}^g$ is selected as a constant matrix as $\hat{B}^g = diag[0.15\ 0.15\ 0.15]$ (kgm^2); this in turn gives $E = 0.6$ (obtained from prior inertia knowledge of the cCub [33]) according to Assumption 2. Due to symmetry in the mechanical structure of both legs of cCub, we only present the experimental results for the right leg.

A. Experiments of Scenario S1 and Results

1) Experimental Scenario S1: This scenario studies the capability of the proposed ASMC to cope with desired trajectory having different speeds. For this purpose, five different periodic desired trajectories, all generated using a fifth-order polynomial and having different speeds are selected as in Fig. 6. It can be noticed from Fig. 6 that the desired position angles span $\pm 10, \pm 15, \pm 20, \pm 25$ and ± 30 degrees within 5sec; accordingly, we call five experiments using these five different desired trajectories as exp-1, exp-2, exp-3, exp-3, exp-4 and exp-5, respectively. For all the experiments, the initial configuration is set as $q_1(0) = -5$, $q_2(0) = +5$, $q_3(0) = -5$ (in degrees). For simplicity, no external disturbances are considered in this scenario by keeping the robot hung in the air (i.e., no ground contact was made).

2) Results and Discussion: The tracking performance of the proposed ASMC for all the three joints are tabulated in Table I in terms of root mean squared error (RMSE) and normalized

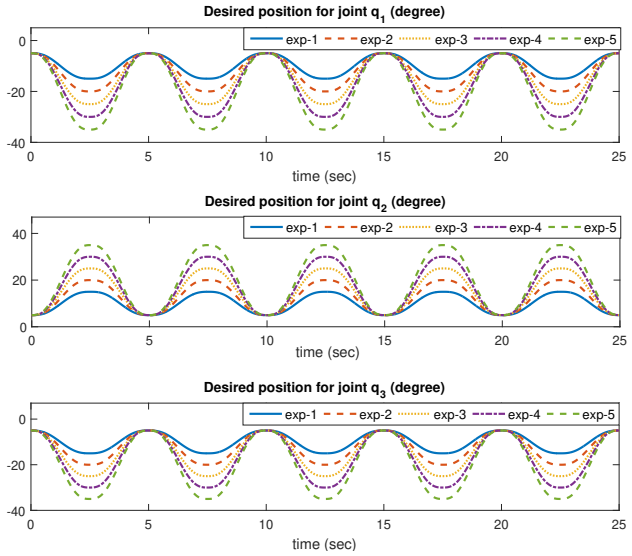

Figure 6. Desired trajectories for the three pitch joints.

Table I
RMSE AND NMAE OF THE PROPOSED ASMC FOR SCENARIO S1

RMSE (degree)					
Joints	exp-1	exp-2	exp-3	exp-4	exp-5
q_1	0.112	0.136	0.157	0.172	0.202
q_2	0.103	0.122	0.137	0.151	0.166
q_3	0.145	0.168	0.184	0.209	0.227
NMAE					
q_1	0.011	0.010	0.009	0.009	0.008
q_2	0.009	0.008	0.008	0.006	0.007
q_3	0.014	0.012	0.011	0.009	0.008

maximum absolute error (NMAE), where normalization is performed with respect to the absolute maximum value of the desired trajectory. Due to lack of space, only the results from exp-5 with the fastest trajectory, i.e., under the worst condition, are plotted in Figs. 7 and 8 in terms of tracking performance and evolutions of overall switching gain and sliding variable, respectively. Table I reveals that the increasing RMSE of the tracking error is simply due to the larger span of the desired trajectories: in fact, the NMAE is quite uniform for all experiments. These observations highlight the effectiveness of the proposed ASMC even while tracking varying desired trajectories.

B. Experiments of Scenario S2 and Results

1) Experimental Scenario S2: In this scenario, the robustness property of the proposed ASMC is verified in the presence of dynamic external disturbances. In fact, in this scenario the robot is required to follow the desired trajectories of exp-2 (cf. Fig. 6) during a combination of the following three phases as shown in Fig. 9:

(i) Phase 1 ($0 \leq t < 9$): in this phase, the robot was hung in the air while following the desired trajectory and at $t = 9$s (approximately) the robot was put on the ground initiating Phase 2;

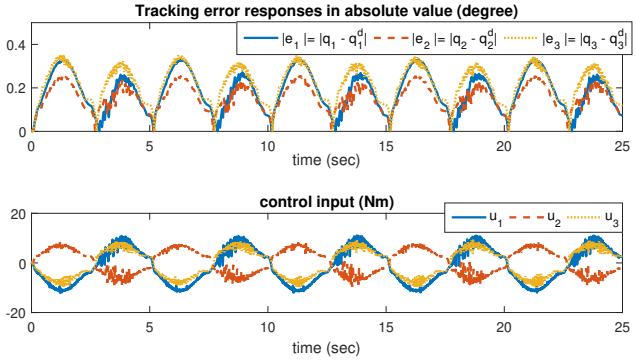

Figure 7. Performance of the proposed ASMC for exp-5.

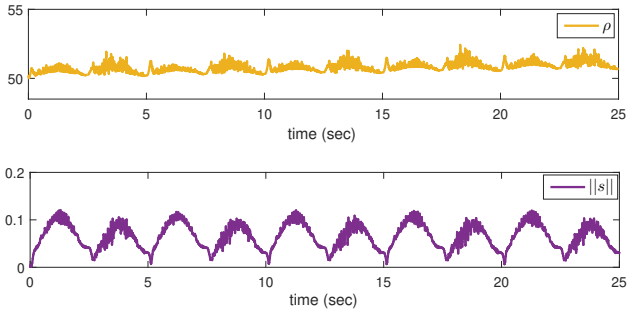

Figure 8. Evolution of the overall switching gain ρ and sliding variable for the proposed ASMC in exp-5 of scenario S1.

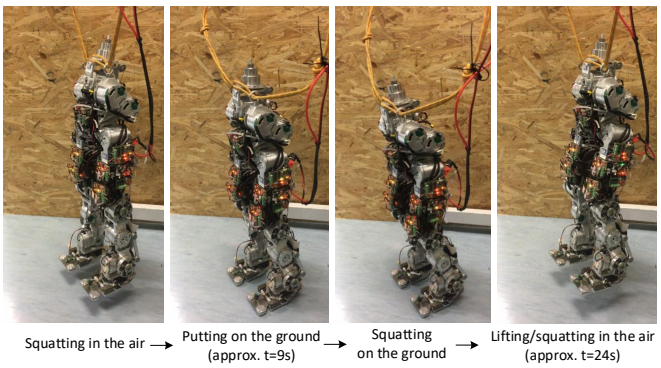

Figure 9. The snapshots of the robustness test of the proposed controller under the Scenario S2.

(ii) Phase 2 ($9 \leq t < 24$): during this phase, a squat like motion was generated by the robot when following the desired trajectory. As the robot's feet is now in contact with the ground, the ground reaction force gets propagated throughout its body and act as a highly nonlinear external disturbance during the postural changes; and

(iii) Phase 3 ($t \geq 24$): in this phase, the robot was again lifted from the ground at around $t = 24$s and thereby, the ground reaction force was suddenly eliminated.

2) Results and Discussion: The tracking performance of the proposed ASMC for this scenario is illustrated in Fig. 10 and evolution of its switching gains and sliding variables are depicted in Fig. 11. Further, to effectively analyse the ability of the proposed scheme in dealing with dynamic disturbances,

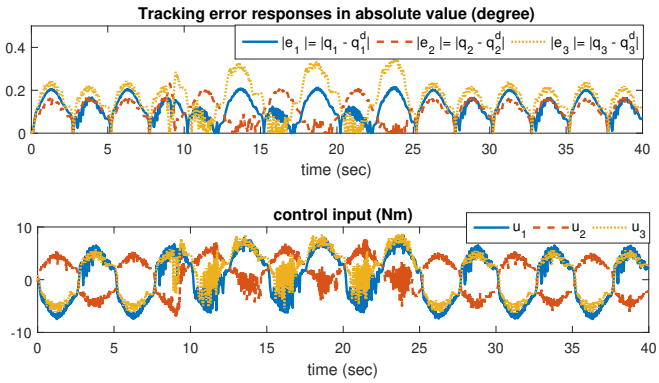

Figure 10. Performance of the proposed ASMC for scenario S2.

Table II
RMSE AND NMAE OF THE PROPOSED ASMC FOR SCENARIO S2

Joints	Phase 1 ($t < 9$)	Phase 2 ($9 \leq t < 24$)	Phase 3 ($t > 24$)
	RMSE (degree)		
q_1	0.135	0.137	0.132
q_2	0.121	0.119	0.117
q_3	0.168	0.194	0.170
	NMAE		
q_1	0.010	0.011	0.010
q_2	0.009	0.010	0.008
q_3	0.012	0.017	0.012

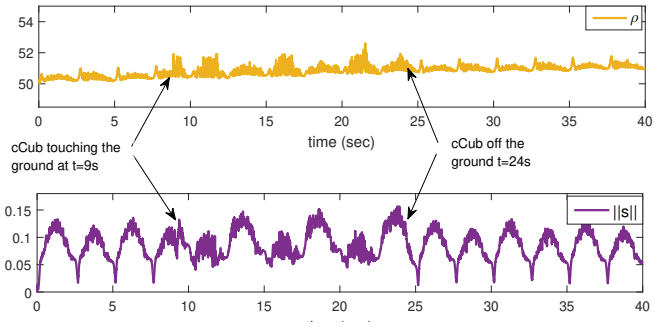

Figure 11. Evolution of the overall switching gain ρ and sliding variable for the proposed ASMC during scenario S2.

its performance is tabulated in Table II in terms of RMSE and NMAE.

It can be noted from Fig. 10 as well as from Table II that, during Phase 2 when the external disturbance was active, the performance of ASMC slightly dipped compared to the other phases. Figure 11 reveals that $||s||$ and ρ are higher during Phase 2 compared to other phases. Interestingly, a sudden spike and a sudden fall can be observed in the plots of Fig. 11 at $t = 9$s and at $t = 24$s, denoting the sudden appearance and removal of disturbances stemming from the effects of cCub's feet touching and being lifted off the ground, respectively. Further, comparing performance of ASMC in Phases 1 and 3 with that of under similar condition in scenario S1 (i.e., exp-2) from Tables I and II, one can realize that ASMC has good *repeatability* and thus, uniformity (i.e., performances are almost similar under same operational condition). Such characteristic is always desirable for a control scheme under practical circumstances.

V. CONCLUSIONS

A novel ASMC law was proposed in this paper that can overcome the over- and under-estimation problems of switching gain without any *a priori* constant upper-bound assumption on the system uncertainty. Comparative simulation study with a 2-link manipulator and experimental results using a multiple degrees-of-freedom biped robot have validated the effectiveness of the proposed control law under various unknown uncertainties. An exciting and challenging future work would be to extend the proposed control law to higher order sliding mode control.

REFERENCES

[1] J. Fei and H. Ding, "Adaptive sliding mode control of dynamic system using rbf neural network," *Nonlinear Dynamics*, vol. 70, no. 2, pp. 1563–1573, 2012.
[2] Y. Zhu and J. Fei, "Disturbance observer based fuzzy sliding mode control of pv grid connected inverter," *IEEE Access*, vol. 6, pp. 21 202–21 211, 2018.
[3] S. Hou and J. Fei, "Finite-time adaptive fuzzy-neural-network control of active power filter," *IEEE Transactions on Power Electronics*, 2019.
[4] Z. Liu, H. Su, and S. Pan, "A new adaptive sliding mode control of uncertain nonlinear systems," *Asian Journal of Control*, vol. 16, no. 1, pp. 198–208, 2014.
[5] C.-Y. Chen, T.-H. S. Li, Y.-C. Yeh, and C.-C. Chang, "Design and implementation of an adaptive sliding-mode dynamic controller for wheeled mobile robots," *Mechatronics*, vol. 19, no. 2, pp. 156–166, 2009.
[6] A. Nasiri, S. K. Nguang, A. Swain, and D. Almakhles, "Passive actuator fault tolerant control for a class of MIMO nonlinear systems with uncertainties," *International Journal of Control*, pp. 1–12, 2017.
[7] A. Nasiri, S. K. Nguang, and A. Swain, "Adaptive sliding mode control for a class of MIMO nonlinear systems with uncertainties," *Journal of the Franklin Institute*, vol. 351, no. 4, pp. 2048–2061, 2014.
[8] Q. Meng, T. Zhang, X. Gao, and J.-y. Song, "Adaptive sliding mode fault-tolerant control of the uncertain stewart platform based on offline multibody dynamics," *IEEE/ASME Transactions on Mechatronics*, vol. 19, no. 3, pp. 882–894, 2014.
[9] S. Liu, H. Zhou, X. Luo, and J. Xiao, "Adaptive sliding fault tolerant control for nonlinear uncertain active suspension systems," *Journal of the Franklin Institute*, vol. 353, no. 1, pp. 180–199, 2016.
[10] S. Mobayen, "An adaptive chattering-free PID sliding mode control based on dynamic sliding manifolds for a class of uncertain nonlinear systems," *Nonlinear Dynamics*, vol. 82, no. 1-2, pp. 53–60, 2015.
[11] S. Roy and S. Baldi, "A simultaneous adaptation law for a class of nonlinearly-parametrized switched systems," *IEEE Control Systems Letters*, vol. 3, no. 3, pp. 487–492, 2019.
[12] T. L. Fernando, H. M. Trinh, and L. Jennings, "Functional observability and the design of minimum order linear functional observers," *IEEE Transactions on Automatic Control*, vol. 55, no. 5, pp. 1268–1273, 2010.
[13] P. Srivastava, S. Singh, and S. Janardhanan, "Linear functional observers for unforced multi-output nonlinear systems," in *IFAC-PapersOnLine, 3th IFAC conference on advances in control and optimization of dynamical systems ACODS 2018*, 2018, pp. 740–744.
[14] S. Roy, I. N. Kar, J. Lee, and M. Jin, "Adaptive-robust time-delay control for a class of uncertain euler–lagrange systems," *IEEE Transactions on Industrial Electronics*, vol. 64, no. 9, pp. 7109–7119, 2017.
[15] M. Jin, S. H. Kang, P. H. Chang, and J. Lee, "Robust control of robot manipulators using inclusive and enhanced time delay control," *IEEE/ASME Transactions on Mechatronics*, vol. 22, no. 5, pp. 2141–2152, 2017.
[16] S. Roy, J. Lee, and S. Baldi, "A new continuous-time stability perspective of time-delay control: Introducing a state-dependent upper bound structure," *IEEE Control Systems Letters*, vol. 3, no. 2, pp. 475–480, 2019.

[17] B. Bandyopadhyay, S. Janardhanan, and S. K. Spurgeon, *Advances in sliding mode control*. Springer, 2013.
[18] F. Plestan, Y. Shtessel, V. Bregeault, and A. Poznyak, "New methodologies for adaptive sliding mode control," *International Journal of Control*, vol. 83, no. 9, pp. 1907–1919, 2010.
[19] ——, "Sliding mode control with gain adaptation–application to an electropneumatic actuator," *Control Engineering Practice*, vol. 21, no. 5, pp. 679–688, 2013.
[20] J. Zhu and K. Khayati, "On a new adaptive sliding mode control for MIMO nonlinear systems with uncertainties of unknown bounds," *International Journal of Robust and Nonlinear Control*, vol. 27, no. 6, pp. 942–962, 2017.
[21] B. Cong, Z. Chen, and X. Liu, "On adaptive sliding mode control without switching gain overestimation," *International Journal of Robust and Nonlinear Control*, vol. 24, no. 3, pp. 515–531, 2014.
[22] Y. Shtessel, M. Taleb, and F. Plestan, "A novel adaptive-gain supertwisting sliding mode controller: Methodology and application," *Automatica*, vol. 48, no. 5, pp. 759–769, 2012.
[23] V. I. Utkin and A. S. Poznyak, "Adaptive sliding mode control with application to super-twist algorithm: Equivalent control method," *Automatica*, vol. 49, no. 1, pp. 39–47, 2013.
[24] J. A. Moreno, D. Y. Negrete, V. Torres-González, and L. Fridman, "Adaptive continuous twisting algorithm," *International Journal of Control*, vol. 89, no. 9, pp. 1798–1806, 2016.
[25] S. Roy, S. B. Roy, and I. N. Kar, "A new design methodology of adaptive sliding mode control for a class of nonlinear systems with state dependent uncertainty bound," in *2018 15th International Workshop on Variable Structure Systems (VSS)*. IEEE, 2018, pp. 414–419.
[26] R. Ortega, J. A. L. Perez, P. J. Nicklasson, and H. J. Sira-Ramirez, *Passivity-based control of Euler-Lagrange systems: mechanical, electrical and electromechanical applications*. Springer Science & Business Media, 2013.
[27] M. W. Spong and M. Vidyasagar, *Robot dynamics and control*. John Wiley & Sons, 2008.
[28] W. Shang and S. Cong, "Motion control of parallel manipulators using acceleration feedback," *IEEE Transactions on Control Systems Technology*, vol. 22, no. 1, pp. 314–321, 2014.
[29] T.-Y. Choi, B.-S. Choi, and K.-H. Seo, "Position and compliance control of a pneumatic muscle actuated manipulator for enhanced safety," *IEEE Transactions on Control Systems Technology*, vol. 19, no. 4, pp. 832–842, 2011.
[30] S. Roy, S. B. Roy, and I. N. Kar, "Adaptive–robust control of Euler–Lagrange systems with linearly parametrizable uncertainty bound," *IEEE Transactions on Control Systems Technology*, vol. 26, no. 5, pp. 1842–1850, 2018.
[31] J. Wu, J. Huang, Y. Wang, and K. Xing, "Nonlinear disturbance observer-based dynamic surface control for trajectory tracking of pneumatic muscle system." *IEEE Trans. Contr. Sys. Techn.*, vol. 22, no. 2, pp. 440–455, 2014.
[32] Q. Xu, "Precision motion control of piezoelectric nanopositioning stage with chattering-free adaptive sliding mode control," *IEEE Transactions on Automation Science and Engineering*, vol. 14, no. 1, pp. 238–248, 2017.
[33] N. G. Tsagarakis, Z. Li, J. Saglia, and D. G. Caldwell, "The design of the lower body of the compliant humanoid robot cCub," in *Robotics and Automation (ICRA), 2011 International Conference on*. IEEE, 2011, pp. 2035–2040.
[34] J.-J. E. Slotine, W. Li *et al.*, *Applied nonlinear control*. Prentice hall Englewood Cliffs, NJ, 1991, vol. 199, no. 1.
[35] H. K. Khalil and J. Grizzle, *Nonlinear systems*. Prentice hall Upper Saddle River, NJ, 2002, vol. 3.
[36] W. Rudin *et al.*, *Principles of mathematical analysis*. McGraw-hill New York, 1976, vol. 3, no. 4.2.
[37] G. Lai, Z. Liu, Y. Zhang, C. P. Chen, and S. Xie, "Adaptive backstepping-based tracking control of a class of uncertain switched nonlinear systems," *Automatica*, vol. 91, pp. 301–310, 2018.

PLACE PHOTO HERE

Author 1 Biography text here.

PLACE PHOTO HERE

Author 2 Biography text here.

PLACE PHOTO HERE

Author 3 Biography text here.

PLACE PHOTO HERE

Author 4 Biography text here.